Spatial Correlation Variability in Multiuser Systems

Spatial Correlation Variability in Multiuser Systems

Harsh Tataria*, Peter J. Smith†, Andreas F. Molisch‡, Seun Sangodoyin‡, Michail Matthaiou*,
Pawel A. Dmochowski§, Jianzhong Zhang¶, and Reiner S. Thomä‖
*Institute of Electronics, Communications and Information Technology (ECIT), Queen's University Belfast, Belfast, U.K.
†School of Mathematics and Statistics, Victoria University of Wellington, Wellington, New Zealand
‡Department of Electrical Engineering, University of Southern California, Los Angeles, CA, USA
§School of Engineering and Computer Science, Victoria University of Wellington, Wellington, New Zealand
¶Mobility and Innovation Laboratory, Samsung Electronics America, Richardson, TX, USA
‖Institut für Informationstechnik, Technische Universität Ilmenau, Ilmenau, Germany
e–mail:{h.tataria, m.matthaiou}@qub.ac.uk, peter.smith@vuw.ac.nz, {molisch, sangodoy}@usc.edu,
pawel.dmochowski@ecs.vuw.ac.nz, jianzhong.z@samsung.com, reiner.thomae@tu-ilmenau.de

***Abstract*—Spatial correlation across an antenna array is known to be detrimental to the terminal signal–to–interference–plus–noise–ratio (SINR) and system spectral efficiency. For a downlink multiuser multiple–input multiple–output system (MU–MIMO), we show that the widely used, yet overly simplified, correlation models which generate fixed correlation patterns for all terminals tend to underestimate the system performance. This is in contrast to more sophisticated, yet physically motivated, remote scattering models that generate variations in the correlation structure across multiple terminals. The remote scattering models are parameterized with measured data from a recent 2.53 GHz urban macrocellular channel measurement campaign in Cologne, Germany. Assuming spatially correlated Ricean fading, with maximum–ratio transmission precoding, tight closed–form approximations to the expected (average) SINR, and ergodic sum spectral efficiency are derived. The expressions provide clear insights into the impact of variable correlation patterns on the above performance metrics. Our results demonstrate the sensitivity of the MU–MIMO performance to different correlation models, and provide a cautionary tale of its impact.**

I. Introduction

In multiuser multiple–input multiple–output (MU–MIMO) systems, an antenna array at a cellular base station (BS) serves a multiplicity of user terminals [1]. Electromagnetic propagation between the array and the terminals is typically characterized by the deterministic far–field specular wavefronts, superimposed on a set of diffuse multipath components (MPCs) [2]. Depending on the severity of scattering and the relative physical separation of two terminals, the MPCs often arrive at two terminals via the same clusters of scatterers, and thus are spatially correlated. Indeed, it is well known in the MU–MIMO literature, that spatial correlation is detrimental to the signal–to–interference–plus–noise–ratio (SINR) of a given terminal, and the system spectral efficiency (see e.g., [3–7]). In fact, this finding is routinely reported when each terminal in the system has a fixed (common) correlation structure.

In sharp contrast to the above statement, a different line of investigations has identified that correlation can enhance MU–MIMO performance [8–11]. The critical observation from these studies is that the departing spread of energy from the BS can arrive at a given terminal via a (partially) different set of clusters located within the vicinity of the terminal. This contributes to variations in the statistics of the channels seen by the terminals. Fundamentally, such variations dependent on the geometry of local scattering, as well as the antenna spacing at the BS. To capture the above physical manifestations, remote scattering models, such as one–ring correlation, have been proposed [8–11]. These models are characterized in terms of the mean azimuth angle–of–arrival (AoA) at a terminal, departing azimuth angular spread, as well as the antenna spacing at the BS. The work of [8, 10] utilized the one–ring model to group the terminals with similar correlation characteristics. Moreover, [11] reports that if the terminal correlation matrices span orthogonal subspaces, the fundamental impairment of pilot contamination vanishes.

Nevertheless, all of the above studies neglect the presence of line–of–sight (LoS) components with correlated diffuse MPCs. Moreover, it remains to be seen just how much performance gain is available with variable correlation, in comparison to the case when each terminal has the same correlation matrix. Even more critically, almost all of the analytical results predicting MU–MIMO performance with linear signal processing and variable correlation, are left in terms of numerical fixed point algorithms, making it extremely difficult to gain any practical insights (see e.g., [7, 9, 10, 12]). To gain a fundamental understanding of MU–MIMO performance with and without variable correlation, it is desirable to have a set of insightful and simple downlink performance metrics. This is missing from the current literature, and in this paper we close this gap. As the remote scattering models rely on spatial parameters of the propagation channel, for most accurate parameterization, we extract the required parameters from a recent 2.53 GHz MU–MIMO measurement campaign in Cologne, Germany. To the best of the authors' knowledge, there are very few studies which use measured multipath parameters to investigate the variability of correlation in multiuser systems. We note that the authors in [2, 13] make initial investigations into characterizing the commonality of scattering clusters along with the LoS components at different terminal locations.

Specifically, our main contributions are as follows:

- We derive closed–form approximations to the expected per–terminal SINR and ergodic sum spectral efficiency with maximum–ratio transmission (MRT) precoding. Assuming spatially correlated Ricean fading, the approximations provide clear insights into the impact of various system parameters, such as the number of BS antennas, unequal correlation structure, Ricean K–factor, and

average downlink signal–to–noise–ratio (SNR). To the best of the authors' knowledge, such general, and simple analyses are missing from the literature.

- We prove that for a fixed average correlation matrix for all terminals, equal correlation increases the expected interference power, in contrast to variable correlation. As a result, equal correlation provides a useful lower limit on the performance of such systems.
- Our numerical findings suggest that the choice of a particular correlation model has a significant impact on the expected SINR and ergodic spectral efficiency. Physically motivated models, such as one–ring, give enhanced performance over non–physical models, such as the exponential and Clerckx correlation models [14]. To parameterize the one–ring model, we utilize measured angular spreads and mean AoA distributions at 2.53 GHz from a recent urban macrocellular (UMa) measurement campaign in Cologne. It is shown that the azimuth angular spread can be modeled as a Gaussian random variable, while the mean AoA follows a uniform distribution.

Notation. Upper and lower boldface letters represent matrices and vectors. The $M \times M$ identity matrix is denoted as $\mathbf{I}_M$. Transpose, Hermitian transpose, inverse and trace operators are denoted by $(\cdot)^{\mathrm{T}}$, $(\cdot)^{\mathrm{H}}$, $(\cdot)^{-1}$, and $\mathrm{tr}\{\cdot\}$, respectively. $||\cdot||_{\mathrm{F}}$ and $|\cdot|$ denote the Frobenius and scalar norms. We use $\mathbf{h} \sim \mathcal{CN}(\mathbf{m}, \mathbf{Q})$ to denote a complex Gaussian distribution for $\mathbf{h}$ with mean $\mathbf{m}$ and covariance matrix $\mathbf{Q}$. Similarly, $h \sim \mathcal{U}[a, b]$ is used to denote a uniform random variable for h taking on values from a to b. Finally, $\mathbb{E}\{\cdot\}$ denotes the statistical expectation of a random variable.

II. System and Propagation Models

We consider the downlink of a single–cell MU–MIMO system in an UMa environment. The BS is located at the center of a circular cell with radius $\mathrm{R_c}$ and is equipped with a ULA of M transmit antennas. The BS simultaneously serves L single–antenna terminals ($M \geq L$) in the same time–frequency resource. Channel knowledge is assumed at the BS with narrow–band transmission and uniform power allocation. For the remainder of the paper, without loss of generality, terminal 1 will be considered as the desired terminal, while terminals $2, 3, \ldots, L$ are considered as interfering terminals.

A. Propagation Model

The $1 \times M$ propagation channel to terminal 1 from the BS array is assumed to follow a spatially correlated Ricean fading distribution, and is denoted by

$$\mathbf{h}_1 = \sqrt{\frac{K_1}{K_1+1}}\widehat{\mathbf{h}}_1 + \sqrt{\frac{1}{1+K_1}}\widetilde{\mathbf{h}}_1\mathbf{R}_1^{\frac{1}{2}} = \underbrace{\widehat{\kappa}_1\widehat{\mathbf{h}}_1}_{\mathbf{v}_1} + \underbrace{\widetilde{\kappa}_1\widetilde{\mathbf{h}}_1\mathbf{R}_1^{\frac{1}{2}}}_{\mathbf{w}_1}. \quad (1)$$

Note that the $1 \times M$ specular and diffuse MPCs are denoted by $\mathbf{v}_1$ and $\mathbf{w}_1$, respectively. Moreover, K_1 denotes the ratio between the power of the specular and diffuse MPCs for terminal 1, and is known as the Ricean K–factor. Note that K_1 is unique to terminal 1, and is a function of the local scattering in its proximity. Further to this, $\widetilde{\mathbf{h}}_1 \sim \mathcal{CN}(0, \mathbf{I}_M)$, $\widehat{\mathbf{h}}_1 = [1, e^{j2\pi d\cos(\phi_1)}, \ldots, e^{j2\pi d(M-1)\cos(\phi_1)}]$. Here d is the antenna spacing between successive elements normalized by λ, the wavelength associated with the operating carrier frequency, f_{c}. Note that ϕ_1 is the azimuth angle–of–departure (AoD) for terminal 1. In addition to the LoS components, we consider correlated MPCs. To this end, unlike previous works (see e.g., [3–7]), we define a $M \times M$ spatial correlation matrix for terminal 1 as $\mathbf{R}_1$. Naturally, $\mathbf{R}_1$ is a function of the spatial parameters of the propagation channel, such as the angular spread and the mean AoA [8–11, 13]. Further discussion on the possible structures of $\mathbf{R}_1$ is given in Section V.

B. Downlink Received Signal Model

The received signal at terminal 1 can be written as

$$y_1 = \sqrt{\frac{\beta_1}{\eta}}\mathbf{h}_1\mathbf{g}_1 s_1 + \sum_{i=2}^{L}\sqrt{\frac{\beta_1}{\eta}}\mathbf{h}_1\mathbf{g}_i s_i + n_1, \quad (2)$$

where β_1 denotes the received power at terminal 1 from the BS (discussed later in the text). Moreover, $\mathbf{g}_1$ is the $M \times 1$ un–normalized downlink precoding vector from the BS array to terminal 1, obtained from column 1 of $\mathbf{G}$, the composite $M \times L$ un–normalized precoding matrix. The data symbol for terminal 1 is denoted by s_1, such that $\mathbb{E}\{|s_1|^2\} = 1$, and $n_1 \sim \mathcal{CN}(0, \sigma^2)$ models the additive white Gaussian noise at terminal 1. Note that σ^2 is fixed for all terminals $1, 2, \ldots, L$. Following [3], $\eta = \|\mathbf{G}\|_{\mathrm{F}}^2/L$ is the precoding normalization parameter such that $\mathbb{E}\{\|\mathbf{g}_\ell\|^2\} = 1$, for $\ell = 1, 2, \ldots, L$ (discussed further in the text). This ensures that the average transmit power at the BS remains unchanged. The received power at terminal 1, $\beta_1 = \rho A \zeta_1 (r_0/r_1)^\alpha$ is composed of the average downlink transmit power, ρ, with large–scale propagation effects. In particular, A is the unit–less constant for geometric attenuation at a reference distance r_0, r_1 is the link distance between the BS and terminal 1, α is the attenuation exponent and ζ_1 models the effects of shadow fading which follows a lognormal distribution, i.e., $10\log_{10}(\zeta_1) \sim \mathcal{N}(0, \sigma_{\mathrm{sh}}^2)$. For the rest of the paper, we assume that $\sigma^2 = 1$. Thus, the average downlink SNR is equivalent to the average downlink transmit power, $\rho/\sigma^2 = \rho$. In line with [15], we employ a probability based approach to determine if a given terminal experiences LoS or non LoS (NLoS) propagation. The LoS and NLoS probabilities are a function of the link distance, from which the LoS and NLoS geometric attenuation and other link characteristics are obtained. The terminal dependent K-factors are assumed to follow a lognormal distribution with the mean and variance provided in [15]. For the sake of consistency, we delay the discussion of the above mentioned approach and other large–scale parameters to Section V.

C. MRT SINR and Ergodic Sum Spectral Efficiency

With MRT, $\mathbf{g}_1 = \mathbf{g}_{1,\mathrm{MRT}} = \mathbf{h}_1^{\mathrm{H}}$, which forms the first column of the composite $M \times L$ MRT precoding matrix, $\mathbf{G}_{\mathrm{MRT}} = \mathbf{H}^{\mathrm{H}}$. Note that $\mathbf{H} = \left[\mathbf{h}_1^{\mathrm{T}}, \mathbf{h}_2^{\mathrm{T}}, \ldots, \mathbf{h}_L^{\mathrm{T}}\right]^{\mathrm{T}}$ is the $L \times M$ composite matrix containing channels for all L terminals. From (2), the MRT SINR for terminal 1 is given by

$$\mathrm{SINR}_{1,\mathrm{MRT}} = \frac{\frac{\beta_1}{\eta_{\mathrm{MRT}}}\left|\mathbf{h}_1\mathbf{g}_{1,\mathrm{MRT}}\right|^2}{\sigma^2 + \frac{\beta_1}{\eta_{\mathrm{MRT}}}\sum_{i=2}^{L}\left|\mathbf{h}_1\mathbf{g}_{i,\mathrm{MRT}}\right|^2}, \quad (3)$$

where $\eta_{\text{MRT}} = \|\mathbf{G}_{\text{MRT}}\|_{\text{F}}^2/L$. The received SINR with MRT in (3) can be translated into an ergodic sum spectral efficiency (in bits/sec/Hz) for all L terminals. This is denoted as

$$\text{R}_{\text{MRT}} = \mathbb{E}\left\{\sum_{\ell=1}^{L}\log_2\left(1+\text{SINR}_{\ell,\text{MRT}}\right)\right\}. \quad (4)$$

In (4), the statistical expectation is performed over an ensemble of the diffuse MPCs in the propagation channel.

III. Analytical Results and Implications

A. Expected MRT SINR and Ergodic Sum Spectral Efficiency

From (3), the expected SINR for terminal 1 can be obtained by computing $\mathbb{E}\{\text{SINR}_{1,\text{MRT}}\}$. Exact evaluation of $\mathbb{E}\{\text{SINR}_{1,\text{MRT}}\}$ is extremely challenging, due to the ratio of expectations [3, 5, 16]. To overcome this difficulty, we employ the commonly used first–order Laplace expansion [3, 16] to approximate $\mathbb{E}\left\{\text{SINR}_{1,\text{MRT}}\right\}$, allowing us to write

$$\mathbb{E}\left\{\text{SINR}_{1,\text{MRT}}\right\} \approx \frac{\frac{\beta_1}{\widehat{\eta}_{\text{MRT}}}\mathbb{E}\left\{\left|\mathbf{h}_1\mathbf{g}_{1,\text{MRT}}\right|^2\right\}}{\sigma^2+\frac{\beta_1}{\widehat{\eta}_{\text{MRT}}}\sum_{i=2}^{L}\mathbb{E}\left\{\left|\mathbf{h}_1\mathbf{g}_{i,\text{MRT}}\right|^2\right\}}. \quad (5)$$

In (5), $\widehat{\eta}_{\text{MRT}} = \mathbb{E}\left\{\eta_{\text{MRT}}\right\}$.

Remark 1. The approximation in (5) is a first–order Laplace expansion, and is of the form $\mathbb{E}\{X/Y\} \approx \mathbb{E}\{X\}/\mathbb{E}\{Y\}$. As shown in [3, 16], the accuracy of such approximations relies on Y having a small variance relative to its mean. This can be seen by applying a multivariate Taylor series to X/Y around $\mathbb{E}\{X\}/\mathbb{E}\{Y\}$. The quadratic forms in (5) are well suited to this approximation, especially when M and L start to grow, since the averaging implicit in the quadratic forms gives the variance reduction required. For further discussion, we refer the interested reader to [3, 16]. In the sequel, the expectations on the numerator and denominator of (5) are derived.

Lemma 1. With a spatially correlated Ricean channel to terminal 1, the expected value of the desired signal power using MRT is given by

$$\delta_1 = \left(\widehat{\kappa}_1\right)^4 M^2 + 2M^2\left(\widetilde{\kappa}_1\right)^2\left(\widehat{\kappa}_1\right)^2 + 2\left(\widetilde{\kappa}_1\right)^2\left(\widehat{\kappa}_1\right)^2\widehat{\mathbf{h}}_1\mathbf{R}_1\widehat{\mathbf{h}}_1^{\text{H}} + \left(\widetilde{\kappa}_1\right)^4\left\{M^2+\text{tr}\left\{\left(\mathbf{R}_1\right)^2\right\}\right\}. \quad (6)$$

Proof: From (1), we know that $\mathbf{h}_1 = \widehat{\kappa}_1\widehat{\mathbf{h}}_1 + \widetilde{\kappa}_1\widetilde{\mathbf{h}}_1\mathbf{R}_1^{\frac{1}{2}} = \mathbf{v}_1 + \mathbf{w}_1$. Then, via first principles, one can state

$$\begin{aligned}\delta_1 &= \mathbb{E}\left\{\left|\mathbf{h}_1\mathbf{g}_{1,\text{MRT}}\right|^2\right\} = \mathbb{E}\left\{\left|\mathbf{h}_1\mathbf{h}_1^{\text{H}}\right|^2\right\}\\ &= \mathbb{E}\left\{\left(\mathbf{v}_1+\mathbf{w}_1\right)\left(\mathbf{v}_1^{\text{H}}+\mathbf{w}_1^{\text{H}}\right)\left(\mathbf{v}_1+\mathbf{w}_1\right)\left(\mathbf{v}_1^{\text{H}}+\mathbf{w}_1^{\text{H}}\right)\right\}. \quad (7)\end{aligned}$$

Expanding (7), taking the expectation over $\widetilde{\mathbf{h}}_1$ in $\mathbf{w}_1$, and simplifying allows one to write

$$\begin{aligned}\delta_1 &= \left(\mathbf{v}_1\mathbf{v}_1^{\text{H}}\right)^2 + 2M\left(\widetilde{\kappa}_1\right)^2\mathbf{v}_1\mathbf{v}_1^{\text{H}}\\ &\quad + 2\left(\widetilde{\kappa}_1\right)^2\mathbf{v}_1\mathbf{R}_1\mathbf{v}_1^{\text{H}} + \left(\widetilde{\kappa}_1\right)^4\mathbb{E}\left\{\left(\widetilde{\mathbf{h}}_1\mathbf{R}_1\widetilde{\mathbf{h}}_1^{\text{H}}\right)^2\right\}. \quad (8)\end{aligned}$$

Via an eigenvalue decomposition, $\mathbf{R}_1 = \mathbf{X}_1\mathbf{\Lambda}_1\mathbf{X}_1^{\text{H}}$, and as a result $\mathbb{E}\{(\widetilde{\mathbf{h}}_1\mathbf{R}_1\widetilde{\mathbf{h}}_1^{\text{H}})^2\} = \mathbb{E}\{\{\sum_{j=1}^{M}[\mathbf{\Lambda}_1]_{j,j}|(\widetilde{\mathbf{h}}_1)_j|^2\}^2\}$. The notation $[\mathbf{\Lambda}_1]_{j,j}$ denotes the (j,j)–th entry of $\mathbf{\Lambda}_1$, and $(\widetilde{\mathbf{h}}_1)_j$ denotes the j–th entry of $\widetilde{\mathbf{h}}_1$. Taking the expectation over $\widetilde{\mathbf{h}}_1$ and simplifying permits us to write $\mathbb{E}\{(\widetilde{\mathbf{h}}_1\mathbf{R}_1\widetilde{\mathbf{h}}_1^{\text{H}})^2\} = (\text{tr}\{\mathbf{R}_1\})^2 + \text{tr}\{(\mathbf{R}_1)^2\}$. Recognizing that $\text{tr}\{\mathbf{R}_1\} = M$,

$$\mathbb{E}\left\{(\widetilde{\mathbf{h}}_1\mathbf{R}_1\widetilde{\mathbf{h}}_1^{\text{H}})^2\right\} = M^2 + \text{tr}\left\{\left(\mathbf{R}_1\right)^2\right\}. \quad (9)$$

Substituting the right–hand side of (9) into δ_1 in (8), recognizing that $\mathbf{v}_1\mathbf{v}_1^{\text{H}} = \left(\widehat{\kappa}_1\right)^2 M$, and extracting the constants gives the desired result in Lemma 1. ∎

Lemma 2. Under the same conditions as Lemma 1, the expected interference power to terminal 1 from transmission to terminal i is given by

$$\begin{aligned}\chi_{1,i} &= \left(\widetilde{\kappa}_1\right)^2\left(\widetilde{\kappa}_i\right)^2\text{tr}\{\mathbf{R}_1\mathbf{R}_i\} + \left(\widetilde{\kappa}_1\right)^2\left(\widehat{\kappa}_i\right)^2\text{tr}\left\{\widehat{\mathbf{h}}_i\mathbf{R}_1\widehat{\mathbf{h}}_i^{\text{H}}\right\}\\ &\quad + \left(\widehat{\kappa}_1\right)^2\left(\widetilde{\kappa}_i\right)^2\text{tr}\left\{\widehat{\mathbf{h}}_1\mathbf{R}_i\widehat{\mathbf{h}}_1^{\text{H}}\right\} + \left(\widehat{\kappa}_1\right)^2\left(\widehat{\kappa}_i\right)^2\left|\widehat{\mathbf{h}}_1\widehat{\mathbf{h}}_i^{\text{H}}\right|^2. \quad (10)\end{aligned}$$

Note that $i = 2, 3, \ldots, L$, and are the interfering terminals.

Proof: Similar to the proof of Lemma 1, we know that $\mathbf{h}_1 = \widehat{\kappa}_1\widehat{\mathbf{h}}_1 + \widetilde{\kappa}_1\widetilde{\mathbf{h}}_1\mathbf{R}_1^{\frac{1}{2}} = \mathbf{v}_1 + \mathbf{w}_1$. This allows us to express the interference to terminal 1 as

$$\chi_{1,i} = \mathbb{E}\left\{\left|\mathbf{h}_1\mathbf{g}_{i,\text{MRT}}\right|^2\right\} = \mathbb{E}\left\{\left(\mathbf{v}_1+\mathbf{w}_1\right)\left(\mathbf{v}_i^{\text{H}}+\mathbf{w}_i^{\text{H}}\right)\right\}. \quad (11)$$

Further expansion and simplifications permits us to write

$$\begin{aligned}\chi_{1,i} &= \mathbb{E}\left\{\mathbf{w}_1\mathbf{w}_i^{\text{H}}\mathbf{w}_i\mathbf{w}_1^{\text{H}}\right\} + \mathbb{E}\left\{\mathbf{w}_1\mathbf{v}_i^{\text{H}}\mathbf{v}_i\mathbf{w}_1^{\text{H}}\right\}\\ &\quad + \mathbb{E}\left\{\mathbf{v}_1\mathbf{w}_i^{\text{H}}\mathbf{w}_i\mathbf{v}_1^{\text{H}}\right\} + \mathbb{E}\left\{\mathbf{v}_1\mathbf{v}_i^{\text{H}}\mathbf{v}_i\mathbf{v}_1^{\text{H}}\right\}. \quad (12)\end{aligned}$$

Noticing that $\mathbb{E}\{\mathbf{w}_i^{\text{H}}\mathbf{w}_i\} = \mathbb{E}\{\widetilde{\kappa}_i\widetilde{\mathbf{h}}_i\mathbf{R}_i^{\frac{1}{2}}\widetilde{\kappa}_i\mathbf{R}_i^{\frac{1}{2}}\widetilde{\mathbf{h}}_i^{\text{H}}\} = (\widetilde{\kappa}_i)^2\mathbf{R}_i$, and substituting back the definitions of $\mathbf{w}_1$, $\mathbf{v}_1$, $\mathbf{w}_i$, and $\mathbf{v}_i$ into (12), and extracting the relevant constants gives

$$\begin{aligned}\chi_{1,i} &= \left(\widetilde{\kappa}_1\right)^2\left(\widetilde{\kappa}_i\right)^2\text{tr}\left\{\mathbf{R}_1\mathbf{R}_i\right\}\\ &\quad + \left(\widetilde{\kappa}_1\right)^2\left(\widehat{\kappa}_i\right)^2\mathbb{E}\left\{\text{tr}\left\{\mathbf{R}_1^{\frac{1}{2}}\widehat{\mathbf{h}}_i^{\text{H}}\widehat{\mathbf{h}}_i\mathbf{R}_1^{\frac{1}{2}}\widetilde{\mathbf{h}}_1^{\text{H}}\widetilde{\mathbf{h}}_1\right\}\right\}\\ &\quad + \left(\widehat{\kappa}_1\right)^2\left(\widetilde{\kappa}_i\right)^2\mathbb{E}\left\{\text{tr}\left\{\widetilde{\mathbf{h}}_i^{\text{H}}\widetilde{\mathbf{h}}_i\mathbf{R}_i^{\frac{1}{2}}\widehat{\mathbf{h}}_1^{\text{H}}\widehat{\mathbf{h}}_1\mathbf{R}_i^{\frac{1}{2}}\right\}\right\}\\ &\quad + \left(\widehat{\kappa}_1\right)^2\left(\widehat{\kappa}_i\right)^2\left|\widehat{\mathbf{h}}_1\widehat{\mathbf{h}}_i^{\text{H}}\right|^2. \quad (13)\end{aligned}$$

Taking the expectation of the traces and simplifying gives the desired result, concluding the proof. ∎

Lemma 3. Under the same condition as Lemmas 1 and 2, $\widehat{\eta}_{\text{MRT}}$ is given by

$$\widehat{\eta}_{\text{MRT}} = \mathbb{E}\left\{\eta_{\text{MRT}}\right\} = M. \quad (14)$$

Proof: By definition, $\widehat{\eta}_{\text{MRT}} = (1/L)\mathbb{E}\{\text{tr}\{\sum_{j=1}^{L}\mathbf{h}_j^{\text{H}}\mathbf{h}_j\}\}$. Substituting $\mathbf{h}_j$ from (1) for any terminal j, taking the expectation over $\widetilde{\mathbf{h}}_j$ and extracting the relevant constants yields the desired result. Note that only a sketch of the proof is given here as it relies on straightforward algebraic manipulations. ∎

Theorem 1. The expected SINR for terminal 1 with MRT processing can be approximated as

$$\mathbb{E}\left\{\text{SINR}_{1,\text{MRT}}\right\} \approx \frac{\frac{\beta_1}{\widehat{\eta}_{\text{MRT}}}\delta_1}{\sigma^2+\frac{\beta_1}{\widehat{\eta}_{\text{MRT}}}\sum_{i=2}^{L}\chi_{1,i}}, \quad (15)$$

where δ_1, $\chi_{1,i}$ and $\widehat{\eta}_{\text{MRT}}$ are as in (6), (10), and (14).

Proof: Substuting Lemmas 1, 2, and 3 for δ_1, $\chi_{1,i}$, and $\widehat{\eta}_{\text{MRT}}$ gives the desired result. ∎

B. Implications of Theorem 1

To the best of the authors' knowledge, the result in Theorem 1 is the first closed–form approximation for an average SINR of an arbitrary terminal, under a fully heterogeneous channel consisting of variable correlation, variable LoS levels, and variable link gains. Several important insights can be obtained by inspecting the individual structures of δ_1 and $\chi_{1,i}$ in Lemmas 1 and 2. It can be seen that both δ_1 and $\chi_{1,i}$ contain quadratic forms of the type $\widehat{\mathbf{h}}_1\mathbf{R}_1\widehat{\mathbf{h}}_1^{\text{H}}$. Via the Rayleigh

quotient result, such quadratic forms are maximized when $\widehat{\mathbf{h}}_1$ is aligned (parallel) with the direction of the maximum eigenvector of $\mathbf{R}_1$. Alignment of the desired LoS component, $\widehat{\mathbf{h}}_1$ with the desired correlation matrix $\mathbf{R}_1$ amplifies the expected signal power. On the other hand, alignment of $\widehat{\mathbf{h}}_i$ with $\mathbf{R}_1$, $\widehat{\mathbf{h}}_1$ with $\mathbf{R}_i$, and $\widehat{\mathbf{h}}_1$ with $\widehat{\mathbf{h}}_i$ increases the expected multiuser interference. In the same fashion, if $\mathbf{R}_1$ and $\mathbf{R}_i$ are aligned, the overall preferential directions of the two propagation channels become similar and degrade the expected SINR. The global phenomenon is that the SINR decreases by virtue of channel similarities of various types (LoS and correlation), and increases if the channels are more diverse. The result in Theorem 1 also lends itself to many special cases, for instance in pure NLoS conditions, with and without variable correlation, as well as under Ricean fading with fixed correlation matrices. Due to space constraints, we omit presenting all possible special cases, but demonstrate an important insight into the impact of variable spatial correlation for fully NLoS (correlated Rayleigh) fading below.

Corollary 1. Under fully NLoS conditions, with unequal MPCs statistics to each terminal, the expected MRT SINR for terminal 1 can be approximated as

$$\mathbb{E}\left\{\text{SINR}_{1,\text{MRT}}\right\} \approx \frac{\frac{\beta_1}{M}\left\{M^2+\text{tr}\left\{\left(\mathbf{R}_1\right)^2\right\}\right\}}{\sigma^2+\frac{\beta_1}{M}\sum_{i=2}^{L}\text{tr}\left\{\mathbf{R}_1\mathbf{R}_i\right\}}. \quad (16)$$

Proof: Setting $\widehat{\kappa}_1 = \widehat{\kappa}_1 = 0$ in Lemmas 1, 2, and 3 yields the desired result. ■

Remark 2. Note that the interference power (second term on the denominator of (16)) can also be written as $(\beta_1/M)(L-1)\text{tr}\{\mathbf{R}_1\mathbf{R}_{-1}\}$, where $\mathbf{R}_{-1} = (\sum_{i=2}^{L}\mathbf{R}_i)/(L-1)$ is the average correlation matrix of all interfering terminals $i = 2, 3, \ldots, L$. While the numerator grows quadratically with increasing M, and the size of $\mathbf{R}_1$, it is straightforward to observe that when $\text{tr}\{\mathbf{R}_1\mathbf{R}_{-1}\}$ increases, the expected interference power also increases. To this end, we study the impact of variation in the correlation structures on the expected SINR derived in (16). The case of variable correlation results in $\mathbf{R}_1 \neq \mathbf{R}_{-1}$. In order to make a fair comparison with the distinct values of $\mathbf{R}_1$ and $\mathbf{R}_{-1}$, for the fixed correlation case, a common value given by $(1/2)(\mathbf{R}_1+\mathbf{R}_{-1})$ is assumed for both correlation matrices. Therefore, the interference term relies on $\text{tr}\{\mathbf{R}_1\mathbf{R}_{-1}\}$ for the variable correlation case, and $\text{tr}\{((1/2)(\mathbf{R}_1+\mathbf{R}_{-1}))^2\}$ for the fixed (common) correlation case. Beginning with the fact that $\text{tr}\{\mathbf{A}^2\} \geq 0$ for any Hermitian matrix $\mathbf{A}$, one can write

$$\text{tr}\left\{\left(\frac{\mathbf{R}_1-\mathbf{R}_{-1}}{2}\right)^2\right\} \geq 0, \quad (17)$$

$$\text{tr}\left\{\frac{\mathbf{R}_1^2}{4}+\frac{\mathbf{R}_{-1}^2}{4}-\frac{\mathbf{R}_1\mathbf{R}_{-1}}{4}-\frac{\mathbf{R}_{-1}\mathbf{R}_1}{4}\right\} \geq 0, \quad (18)$$

$$\text{tr}\left\{\frac{\mathbf{R}_1^2}{4}+\frac{\mathbf{R}_{-1}^2}{4}+\frac{\mathbf{R}_1\mathbf{R}_{-1}}{4}+\frac{\mathbf{R}_{-1}\mathbf{R}_1}{4}-\mathbf{R}_1\mathbf{R}_{-1}\right\} \geq 0, \quad (19)$$

$$\text{tr}\left\{\left(\frac{\mathbf{R}_1+\mathbf{R}_{-1}}{2}\right)^2\right\} \geq \text{tr}\left\{\mathbf{R}_1\mathbf{R}_{-1}\right\}. \quad (20)$$

Fig. 1. BS array view of the UMa site in Cologne.

Fig. 2. Terminal placement in the coverage of the UMa site in Cologne.

Hence, if $\mathbf{R}_1 = \mathbf{R}_{-1}$, the case for fixed (common) correlation matrices, terminal 1 will have a higher total expected interference power in comparison to the variable correlation case where $\mathbf{R}_1 \neq \mathbf{R}_{-1}$. Since this holds across all terminals, it can be concluded that fixed correlation matrices result in the lowest SINR, given a fixed overall average correlation matrix. As a result, such a scenario provides a useful lower bound for the performance of spatially correlated MU–MIMO channels.

We note that (15) can be further translated to approximate the ergodic sum spectral efficiency of the system by

$$\mathbb{E}\left\{\text{R}_{\text{MRT}}\right\} \approx \sum_{\ell=1}^{L}\log_2\left(1+\mathbb{E}\left\{\text{SINR}_{\ell,\text{MRT}}\right\}\right). \quad (21)$$

IV. Propagation Channel Measurements

A. Measurement Environment

The propagation measurements were conducted in the old–town city center in Cologne, a moderate–sized city in Germany with a typical European layout. The investigated area was mostly made up of buildings with similar heights and multiple floors (ranging between 4–8). The BS array (referred to as TX) was mounted on a rooftop of a 30 m high–rise building with the terminals (referred to as RX) placed on the rooftop of a car at approximately 2.5 m above ground. The TX and RX placements in the environment are shown in Figs. 1 and 2. The measurements were conducted in 45 random terminal positions throughout the environment. The TX array was fixed at a given location throughout the measurement campaign. To avoid probable interference at the desired frequencies, the German service provider, Deutsche Telekom, agreed to switch off their BSs operating at the same or adjacent frequencies throughout the duration of the measurements.

B. Measurement Setup

The propagation measurements were performed with a wideband MIMO MEDAV RUSK channel sounder, operating at a center frequency of 2.53 GHz. The RUSK channel sounder is based on the switched array principle, and has been used in a number of previous measurement campaigns (see e.g., [17,

TABLE I
CHANNEL SOUNDER CONFIGURATION

Parameters	Values
Bandwidth	2.52 GHz – 2.54 GHz
No. of frequency points	257
Number of channels	900 × 32
Total time syn. aperture	Approx. 10 mins
Tx ports, Rx ports	900 ports, 32 ports
Azimuth range	$[-180^\circ$ to $180^\circ]$
Elevation range	$[90^\circ$ to $-90^\circ]$

18]). As a result, only a single transmit and receive chains exist. The transmit signal is connected via a fast electronic switch, to the elements of the TX array sequentially. The RX side operates in a similar manner as the TX, allowing for sequential measurement of the propagation channel transfer function between all combinations of TX and RX elements. So long as the measurement sequence occurs within a timescale shorter than the channel coherence time, such a measurement is equivalent to a truly real–time measurement with parallel TX/RX chains for all antenna elements. The precise channel sounder settings are provided in Table I.

The measurement setup utilizes cylindrical array structures at both TX and RX ends of the RUSK sounder. The array structures guarantee a truly 3D (azimuth and elevation) channel measurement and ensures that MPCs from all directions in the urban environment could be easily captured. Both elevation and azimuth parameters are need to be estimated to obtain accurate results, even though in this paper only the azimuth parameters are needed to populate the correlation models. A synthetic array was used at the TX end in the channel sounding setup and was constructed such that an 8–element (2 ports per–element) polarimetric uniform linear patch array (PULPA)[1] was placed on a programmable positioner. The positioner was rotated in the azimuth domain with an angular range from –180° to 180°, in 6 degree step–sizes creating 60 virtual positions and imitating a cylindrical structure. Overall, this results in 60×8×2 TX channels. This is equivalent to a 480 element cylindrical array operating with two polarization states. At the RX, a stacked polarimetric uniform circular patch array (SPUCPA) with 2 (vertical) × 8 (circumference) × 2 (polarization) antenna ports were employed. Further discussion on the above is provided in [19].

C. Parameter Extraction

The RUSK sounder provides a 4–dimensional channel transfer function matrix, $\mathbf{H}(s, f, t, r)$, where s denotes the measurement snapshot index, f is the measured frequency index, while t and r denote TX and RX element indices, respectively. In total, $s = 10$ snapshots were recorded for each measured transfer function to improve the measurement SNR when averaged. The impulse response, of the propagation channel with a given (t, r) pair was obtained via an inverse fast Fourier transform. To extract the spatial parameters of the propagation channel, a high resolution parameter estimation algorithm known as RIMAX was utilized [20]. RIMAX provides a complete double–directional description of the propagation channel and extracts the spatial parameters to obtain an antenna independent characterization of the channel. This means that the spatial parameters of the channel remain independent to the type of the antenna array that is used to make the measurement. Due to space limitations, we omit presenting the procedure for identifying MPCs which belong to a particular clusters of scatterers. More details on this can be found in [19]. Leveraging this property, from the MPCs, we extract the root mean square azimuth angular spread, as well as the mean AoA distributions across all 45 terminal positions. These form the basis for parameterizing the spatial correlation structures considered in the paper (See Section V-A). Even though this is an approximation, it is able to offer significantly greater insights than a purely numerical calculation of the correlation structure, as done routinely in the MU–MIMO literature. The extracted results are presented in Fig. 3 as cumulative distribution functions (CDFs). It can be observed that the azimuth AoD spread has a degree of symmetry and spans over 40°. The variability in the angular spread is due to variability in the local scattering, which can be modeled as $\mathcal{N}(14.02, (6.45^2)^\circ)$ (Gaussian fit on the fig.). In contrast to this, the mean AoA is $\mathcal{U}[-180^\circ, 180^\circ]$ (uniform fit on the fig.), primarily reflecting the distribution of the terminals in the measurement environment.

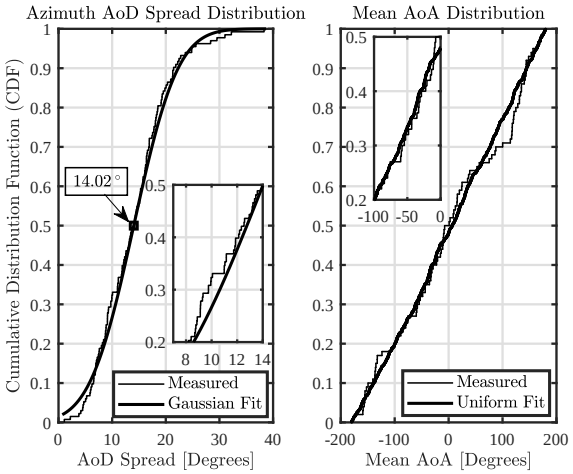

Fig. 3. Measured azimuth AoD and mean AoA CDFs at 2.53 GHz in an UMa environment in Cologne.

V. NUMERICAL RESULTS

Unless otherwise specified, the parameters described below are utilized for all numerical results, and are obtained from [15]. A cell radius, $R_c = 100$ m was chosen with a reference distance $r_0 = 10$ m, such that the terminals are randomly located outside r_0, and inside R_c, following $\mathcal{U}[-180^\circ, 180^\circ]$. The LoS and NLoS attenuation exponents, α, are given by 2.2 and 3.67, respectively. Furthermore, the unit–less constant for geometric attenuation, A, is chosen such that the fifth–percentile of the instantaneous SINR with MRT processing at terminal 1 is 0 dB, when $\rho = 0$ dB with $M = 64$ and $L = 8$.

[1]The PULPA contains more than 8–elements. The other elements are used as dummy elements to assuage fringe effects caused by mutual coupling.

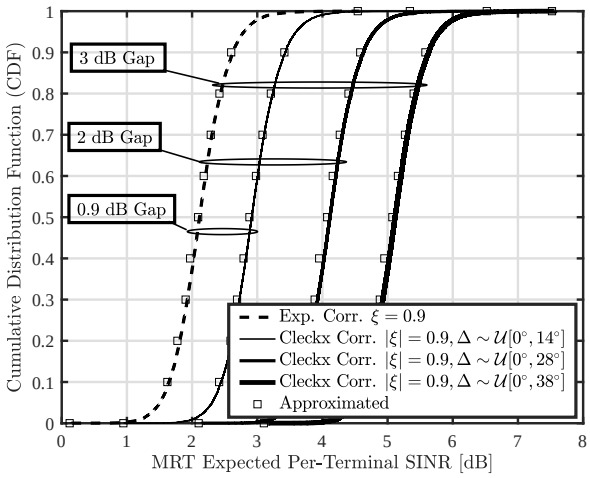

Fig. 4. CDFs of expected SINR with $M = 64$, $L = 8$, and $\rho = 10$ dB.

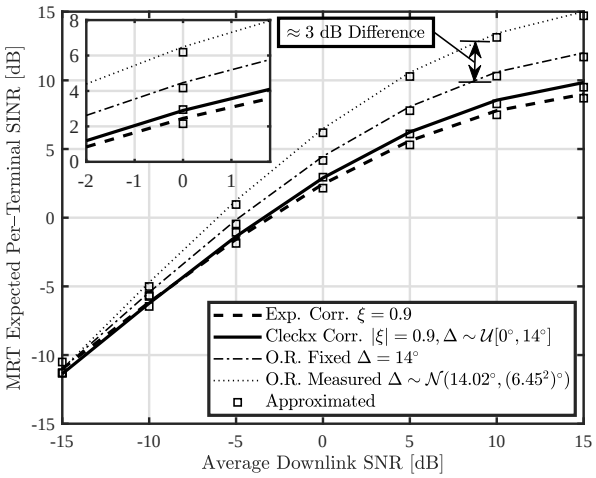

Fig. 5. Expected SINR vs. average downlink SNR with $M = 64$ and $L = 8$.

Note that the exponential correlation model (described further in the section), with the correlation coefficient $\xi = 0.9$, and terminal specific K–factors drawn from a lognormal density with a mean of 9 dB and a standard deviation of 3.5 dB, denoted by $K \sim \ln\left(9, 3.5^2\right)$ dB, were chosen to obtain A. The LoS and NLoS shadow–fading standard deviations, σ_{sh}, are 4 dB and 6 dB. The probability of terminal 1 experiencing LoS is given by $\mathbb{P}_{\text{LoS},1}(r_1) = (\min(18/r_l, 1)(1-e^{-r_1/36}))+e^{-r_1/36}$. Naturally, $\mathbb{P}_{\text{NLoS},1}(r_1) = 1 - \mathbb{P}_{\text{LoS},1}(r_1)$. For each subsequent result, 10^5 Monte–Carlo realizations were generated with an inter–element spacing, $d = 0.5\lambda$ at the BS.

A. Spatial Correlation Models

As a baseline case, we model fixed correlation to each terminal with the widely used exponential model, where the (i, j)–th element of $\mathbf{R}_1$ is expressed as $[\mathbf{R}_1]_{i,j} = \xi^{|i-j|}$, for any i, j in $1, 2, \ldots, M$ with $0 \leq \xi \leq 1$ [3]. Unless otherwise specified, $\xi = 0.9$ is used throughout the evaluation. With variable correlation, we employ two models, namely Clerckx [14], and one–ring (O.R.) [9, 10] correlation. For the Clerckx correlation model, $[\mathbf{R}_1]_{i,j} = \xi_{\text{c}}^{|i-j|}$, where $\xi_{\text{c}} = |\xi| e^{j\Delta_1}$. Here, $|\xi| = \xi$, as in the exponential model, and is the same for each terminal. However, a terminal specific phase, Δ_1, is assumed to be uniformly distributed on a subset of –180° to 180°. This is used to differentiate the terminal locations. In each result, the range of Δ_1 is specified. We refer to the Clerckx model as Clerckx Corr. and the exponential model as Exp. Corr. In contrast to the above, the O.R. model for terminal 1 states $[\mathbf{R}_1]_{i,j} = \frac{1}{2\Delta_1} \int_{-\Delta_1+\phi_0^1}^{\Delta_1+\phi_0^1} e^{-j2\pi d(i,j)\sin(\phi_1)} d\phi_1$, where Δ_1 denotes the azimuth angular spread for terminal 1, ϕ_0^1 denotes the mean AoA, ϕ_1 is the actual AoA, uniformly distributed within the angular spread around the mean AoA. Furthermore, $d(i, j)$ captures the normalized antenna spacing between the i–th and j–th elements. The precise values of Δ_1 for the O.R. model are specified in each subsequent result.

B. Impact of Variable Correlation Structures

Fig. 4 depicts the CDFs of the expected SINR with $M = 64$, $L = 8$, and $\rho = 10$ dB. Each density is obtained by averaging over the diffuse MPCs, with the CDFs representing the variations resulting from the link gains and the K–factors. Two trends can be observed: Firstly, with variable correlation matrices from the Clerckx model, the larger the spread of the random phases in Δ's, the higher the expected SINRs. Despite the correlation magnitude being as high as $\xi = 0.9$, increasing the spread of Δ's to $\mathcal{U}[0, 14°]$, $\mathcal{U}[0, 28°]$, and $\mathcal{U}[0, 38°]$ yields a 0.9, 2, and 3 dB gain in the expected SINR, relative to the exponential correlation case. This performance difference is owed to the fact that increasing the spread of Δ increases the amount of spatial selectivity induced across multiple channels, allowing the composite channel rank to increase. The result demonstrates the sensitivity of multiuser channels to changes in the phase of the correlation matrices. This is in agreement with Remark 2, which predicts higher performance with variable correlation. Secondly, our proposed approximations are tight in comparison to the simulated cases for all Δ values.

Fig. 5 demonstrates the expected SINR as a function of the average received SNR values. Here, in addition to the cases for exponential correlation and Clerckx correlation, the performance with the O.R. model is also evaluated. It can be observed that even with a fixed angular spread, Δ_1, the O.R. model is still able to predict higher expected SINRs in comparison to the Clerckx model, with $\Delta_1 \sim \mathcal{U}[0°, 14°]$. This is due to the fact that both the magnitude and phase of the correlation matrices are variable across each terminal in the case of the O.R. model. The Clerckx correlation matrix assumes a fixed magnitude for each terminal. Moreover, when evaluating the expected SINRs with the measured angular spread values, a 3 dB increase in the SINR is seen at high SNRs (above 5 dB). This is due to the increased variability brought by the random angular spread, which is modeled as a Gaussian random variable from the measured data. The occurrence of larger angular spread values further increases the spatial selectivity of the channel, improving the performance. The impact of the O.R. model is more pronounced in the high SNR regime, where the increasing amounts of scattering in the channel enhances the composite channel rank, and allows the MU–MIMO system to leverage better multiplexing gains. At low SNRs (below –5 dB), where the noise dominates relative to the signal and interference, the impact of variability in

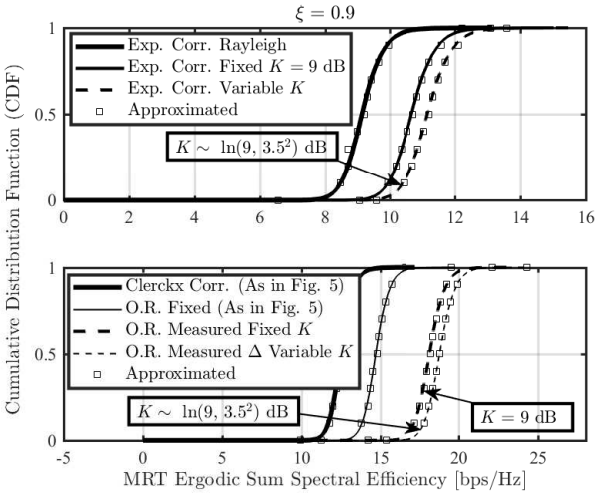

Fig. 6. Ergodic sum spectral efficiency CDFs for various LoS and NLoS scenarios with $M = 64$, $L = 8$ and $\rho = 10$ dB.

correlation plays a less significant role, as the resulting performance from each correlation matrix is almost identical. The proposed approximations are seen to remain tight across all the considered models, and SNR values. This result shows the profound impact variable angular spread has on MU–MIMO systems, and emphasizes that the predicted performance is ultimately governed by the accuracy of the parameterization of different spatial correlation models.

Fig. 6 depicts the CDFs of the ergodic sum spectral efficiency with $M = 64$, $L = 8$, and $\rho = 10$ dB. As shown in the top subfigure, having a dominant specular component leads to a higher ergodic sum spectral efficiency, as it results in an increase in the net expected signal power, while increasing the directivity of the interference. Hence, as long as the terminals have non–overlapping AoAs, the expected interference power is negligible and decreases with increasing LoS strength. For this reason, introducing variability in the K–factors for each terminal yields a further increase in the ergodic sum spectral efficiency due to a larger occurrence of high K values. A similar trend is also seen for the O.R. model in the bottom subfigure, where the aggregate impact of variable K–factors and correlation structures lead to improved performance. In all cases, the derived approximations retain their accuracy, validating the robustness of the simple approximations.

VI. Conclusions

The paper presents closed–form approximations to the expected SINR and ergodic sum spectral efficiency of a MU–MIMO system with MRT precoding. Considering unequally correlated Ricean fading, the analysis is robust to changes in the average downlink SNR, and various physical and non–physical models. It is found that the total expected interference power increases with fixed correlation matrices, degrading the MU–MIMO performance. More physically motivated models, such as the O.R., consider unique magnitude and phases in the correlation matrices for each terminal, and tend to predict higher performance. State–of–the–art UMa propagation measurements are presented at 2.53 GHz to extract the necessary parameters in order to accurately model variable correlation and its impact on MU–MIMO performance. To the best of the authors' knowledge, such an evaluation of a MU–MIMO system is unique and emphasizes that its performance is ultimately governed by the respective correlation model in use.

VII. Acknowledgment

The authors would like to thank Deutsche Telekom for their help in facilitating the measurement campaign. The authors also thank Prof. Larry J. Greenstein for insightful discussions.

References

[1] E. G. Larsson, O. Edfors, F. Tufvesson, and T. L. Marzetta, "Massive MIMO for next generation wireless systems," *IEEE Commun. Mag.*, vol. 52, no. 2, pp. 186-195, Feb. 2014.

[2] X. Gao, O. Edfors, F. Rusek, and F. Tufvesson, "Massive MIMO performance evaluation based on measured propagation data," *IEEE Trans. Wireless Commun.*, vol. 14, no. 7, pp. 3899-3911, Jul. 2015.

[3] H. Tataria, P. J. Smith, and P. A. Dmochowski, "On the general analysis of coordinated regularized zero-forcing precoding: An application to two-tier small-cell networks," *IEEE Trans. Commun.*, vol. 65, no. 7, pp. 3133-3150, Jul. 2017.

[4] H. Falconet, L. Sanguinetti, A. Kammoun, and M. Debbah, "Asymptotic analysis of downlink MISO systems over Rician fading channels," in *Proc. IEEE ICASSP*, May 2016, pp. 3926-3930.

[5] J. Zhang, L. Dai, M. Matthaiou, C. Masouros, and S. Jin, "On the spectral efficiency of space-constrained massive MIMO with linear receivers," in *Proc. of IEEE ICC*, May 2016.

[6] H. Tataria, P. J. Smith, P. A. Dmochowski, and M. Shafi, "General analysis of multiuser MIMO systems with regularized zero-forcing precoding under spatially correlated Rayleigh fading channels," in *Proc. IEEE ICC*, May 2016.

[7] S. Wagner, R. Couillet, M. Debbah, and D. T. M. Slock, "Large system analysis of linear precoding in correlated MISO broadcast channels under limited feedback," *IEEE Trans. Inf. Theory*, vol. 58, no. 7, pp. 4509-4537, Dec. 2012.

[8] J. Nam, G. Caire, and J. Ha, "On the role of transmit spatial correlation diversity in multiuser MIMO systems," *IEEE Trans. Inf. Theory*, vol. 63, no. 1, pp. 336-354, Jan. 2017.

[9] Z. Jiang, A. F. Molisch, G. Caire, and Z. Niu, "Achievable rates of FDD massive MIMO systems with spatial channel correlation," *IEEE Trans. Wireless Commun.*, vol. 14, no. 5, pp. 2868-2882, May 2015.

[10] A. Adhikary, *et al.*, "Joint spatial division and multiplexing for mm-Wave channels," *IEEE J. Sel. Areas Commun.*, vol. 32, no. 6, pp. 1239-1255, Jun. 2014.

[11] E. Bjornsön, J. Hoydis, and L. Sanguinetti, "Pilot contamination is not a fundamental asymptotic limitation in massive MIMO," in *Proc. IEEE ICC*, May 2017.

[12] J. Hoydis, S. ten Brink, and M. Debbah, "Massive MIMO in the UL/DL of cellular networks: How many antennas do we need?," *IEEE J. Sel. Areas Commun.*, vol. 31, no. 2, pp. 160-171, Feb. 2013.

[13] S. L. H. Nguyen, K. Haneda, J. Jarvelainen, A. Karttunen, and J. Putkonen, "On the mutual orthogonality of millimeter-wave massive MIMO channels," in *Proc. IEEE VTC-Spring*, May 2015.

[14] B. Clerckx, G. Kim, and S. Kim, "Correlated fading in broadcast MIMO channels: Curse or blessing?," in *Proc. IEEE GLOBECOM*, Nov. 2008.

[15] 3GPP TR 36.873 v.12.2.0, *Study on 3D channel models for LTE*, 3GPP, Jun. 2015.

[16] Q. Zhang, S. Jin, K.-K. Wong, H. Zhu, and M. Matthaiou, "Power scaling of uplink massive MIMO systems with arbitrary-rank channel means," *IEEE J. Sel. Topics Signal Process.*, vol. 8, no. 5, pp. 966-981, Oct. 2014.

[17] R. S. Thomä, *et al.*, "Identification of time-variant directional mobile radio channels," *IEEE Trans. Instrum. Meas.*, vol. 49, no. 2, pp. 357-364, Apr. 2000.

[18] R. S. Thomä, *et al.*, "MIMO vector channel sounder measurement for smart antenna system evaluation," European Trans. Telecommun., vol. 12, no. 5, pp. 427-438, Sept./Oct. 2001.

[19] S. Sangodoyin, *et al.*, "Cluster-based analysis of 3D MIMO channel measurement in an urban environment," in *Proc. IEEE MILCOM*, Oct. 2015, pp. 744-749.

[20] A. Richter, "Estimation of radio channel parameters: Models and algorithms," Ph.D. dissertation, Technische Universität Ilmenau, Germany, 2005, Available online: www.db-thueringen.de.